IJST, Transactions of Electrical Engineering, Vol. 38, No. E1, pp 1-20
Printed in The Islamic Republic of Iran, 2014

DESIGN AND IMPLEMENTATION OF PRECISE HARDWARE FOR ELECTRICAL IMPEDANCE TOMOGRAPHY (EIT)*

M. KHALIGHI[1**], B. VOSOUGHI VAHDAT[2], M. MORTAZAVI[3] AND M. MIKAEILI[4]

[1]School of Engineering and Science, Sharif University of Technology, International Campus, I. R. of Iran
Email: khalighi58@yahoo.com
[2]School of Engineering and Science, Sharif University of Technology, Tehran, I. R. of Iran
[3]School of Engineering, Islamic Azad University-Abhar Branch, I. R. of Iran
[4]Dept. of Engineering, Biomedical Engineering Group, Shahed University, Tehran, I. R. of Iran

Abstract– Electrical Impedance Tomography (EIT), is one of the safest medical imaging technologies and can be used in industrial process monitoring. In this method, image of electrical conductivity (or electrical impedance) distribution of the inner part of a conductive subject can be reconstructed. The image reconstruction process is done by injecting an accurate current into the boundary of a volume conductor (Ω), measuring voltages around the boundary ($\partial\Omega$) and transmitting them to a computer, and processing on acquired data with software (e.g. MATLAB). The image would be reconstructed from the measured peripheral data by using an iterative algorithm. A precise instrumentation (EIT hardware) plays a very important and vital role in the quality of reconstructed images. In this paper, we have proposed a practical design of a low-cost precise EIT hardware including, a high output impedance VCCS (Voltage-Controlled Current Source) with pulse generation part, precise voltage demodulator and measuring parts, a high performance multiplexer module, and a control unit. All the parts have been practically and accurately tested with successful results, and finally the proposed design was assembled on PCB. The quality of experimental results at the end of this paper, (reconstructed images by using the implemented system), confirms the accuracy of the proposed EIT hardware.

Keywords– EIT, electrical impedance tomography, EIT hardware, EIT instrumentation, EIT current source

1. INTRODUCTION

Electrical Impedance Tomography (EIT) is a relatively new imaging technique. In this method, an image of the inner part of a conductive domain (Ω) can be made with an array of external electrodes which are located on the boundary of domain ($\partial\Omega$). In this imaging method, the image of electrical conductivity (or impedance) distribution of the internal part of a typical conductive subject can be reconstructed [1]. EIT procedure includes injecting an accurate current into the boundary of domain ($\partial\Omega$) via a pair of electrodes, measuring the boundary voltages by means of other electrodes around the boundary and transmitting them to a computer, and at the end, processing the acquired data with software (e.g. MATLAB) to reconstruct the image. Human body tissues contain a wide range of conductivities, and hence the potential exists to use EIT to carry out medical imaging using the conductivity as the parameter to be mapped [2].

As a matter of fact, EIT is a challenging problem. This technique has some advantages compared to other methods, including: simplicity of application, no hazard to the patient (such as X-ray), low cost and portable, and the high speed of data collection and image reconstruction [3]. Although EIT systems suffer

*Received by the editors January 21, 2013; Accepted May 18, 2014.
**Corresponding author

from poor image resolution, the transfer impedances must still be measured with high accuracy. The effect of unknown skin–electrode impedance on measurement errors can also have a significant effect on image quality [4]. EIT still has technical difficulty in terms of developing hardware for data acquisition and the algorithms to reconstruct the images. However, there are some methods to improve imaging quality. The most important of them is hardware improvements to acquire a high-accuracy measured datum [5, 6]. Reconstructed image quality mainly depends on the boundary data accuracy and the reconstruction algorithm [7].

This paper is focused on hardware implementation of EIT. First of all, the top view of our proposed design is illustrated and explained, and each part of the design will be described in detail as well. After that, some experiments done by using the implemented system and their results will be presented. At the end, final reconstructed image of our EIT system will be compared with other works.

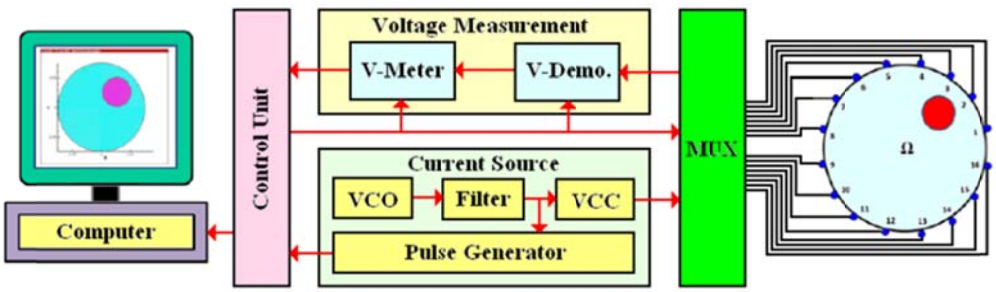

Fig. 1. The main block diagram of proposed EIT hardware design

2. TOP VIEW OF PROPOSED DESIGN

In general, EIT instrumentation comprises digital and analog circuits, an array of electrodes which acts as EIT-sensors and a PC. The image is finally reconstructed from the acquired data (voltages) by using an iterative algorithm. In our design, the analog section of hardware includes an accurate current source and a data acquisition part (to measure voltages with enough precision). The digital part contains control unit. The precision of all units plays a very important role in reconstructed image quality. The top view of the proposed EIT system is illustrated in Fig. 1. The block diagram of the proposed EIT hardware (Fig. 1) has different parts:

1- VCCS (Voltage-Controlled Current Source) which includes a VCO as a waveform generator, a filter, a VCC (Voltage-to-current converter) part, and a pulse generator.
2- Multiplexer module.
3- Control unit.
4- Voltage measurement part containing a voltage demodulator and a voltmeter.

The constant and accurate current produced by the VCCS is injected into the boundary of domain ($\partial\Omega$) via the multiplexer part (MUX). The second task of the current source section is generating two types of pulse train simultaneous with maximum point of positive peaks and zero points of the current waveform. They can be used for sampling of real and imaginary sections of measured voltage in voltage demodulation portion. In order to measure the boundary voltage, meaning demodulating and measuring the electrodes voltage, "V-Demo." and "V-Meter" blocks should be applied respectively after multiplexer block. Control unit is applied for controlling the multiplexer module and measurement parts, and also for communicating with the PC for data transaction. The assembled EIT hardware is shown in Fig. 2.

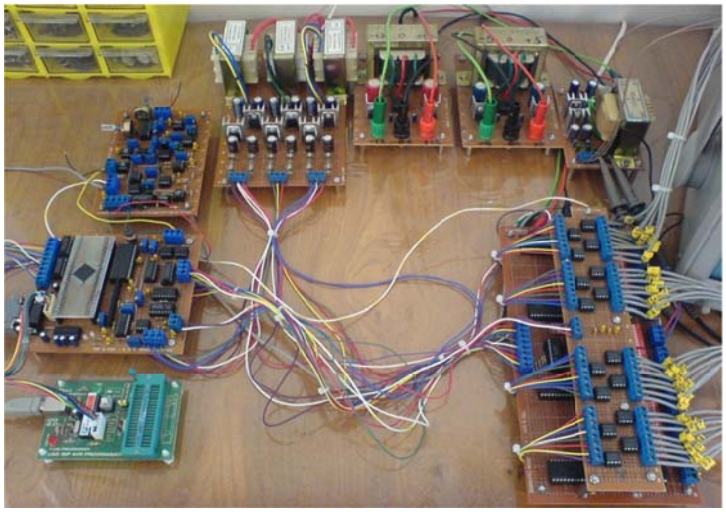

Fig. 2. Assembled EIT hardware

3. VOLTAGE-CONTROLLED CURRENT SOURCE

Electrical Impedance Tomography (EIT) systems require accurate current sources that work over a wide frequency range and with a large variation in load impedance. The simplest technique to obtain a constant current is to use a voltage-controlled current source (VCCS), which can be defined as a combination of positive and negative feedback around a high gain operational or instrumentation amplifier [8]. A typical VCCS used in the EIT systems, consists of waveform generator and Voltage-to-Current Converter (VCC) parts. Design of the VCC in EIT systems is especially important. The VCC part requires stability and high precision, which means that it must have high output impedance. Generally, the waveform used in the EIT systems in most cases is the sinusoidal waveform which is produced by the waveform generation part in digital or analog form [9]. The main features for a typical waveform generator are as follow; an accurate output waveform (i.e. exact sinusoidal waveform without any jitter), a low output impedance (similar to an ideal voltage source), wide operational bandwidth, and steady amplitude over all the frequency range. In addition, the main characteristics for the VCC part to have an excellent VCCS are based on high output impedance, linearity in converting voltage to current, precision of output waveform, supporting a wide range of load, and proper working in a broad range of frequency [10]. The high-performance current source can ameliorate the image quality to a certain extent [11].

The current source in EIT systems must be able to deliver the current over a frequency range between 10KHz and 1MHz and be able to support the load between 100Ω and 10KΩ [9]. Its output impedance must be in the range of more than 100KΩ as well [12], therefore an excellent current source design should satisfy the above conditions. Figure 3 shows the flowchart of the proposed VCCS. It consists of a VCO (Voltage-Controlled Oscillator) part, a Butterworth band-pass filter (Butterworth low-pass and high-pass filters in serial connection), and a VCC (Voltage-to-Current Converter) part.

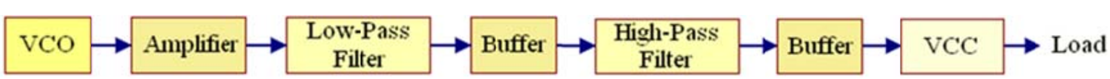

Fig. 3. Flowchart of proposed VCCS design

a) Waveform generation

Schematic circuit of the waveform generation part is shown in Fig. 4. As it can be seen, XR-2206 (EXAR Inc.) has been used in the waveform oscillator part as a VCO. An AD844 IC has been placed at the output of the VCO, to amplify the sinusoidal waveform and also to create a low output impedance value at the output of waveform generation part (measured output impedance of the circuit without AD844, is about 690Ω and with this IC, is about 14Ω).

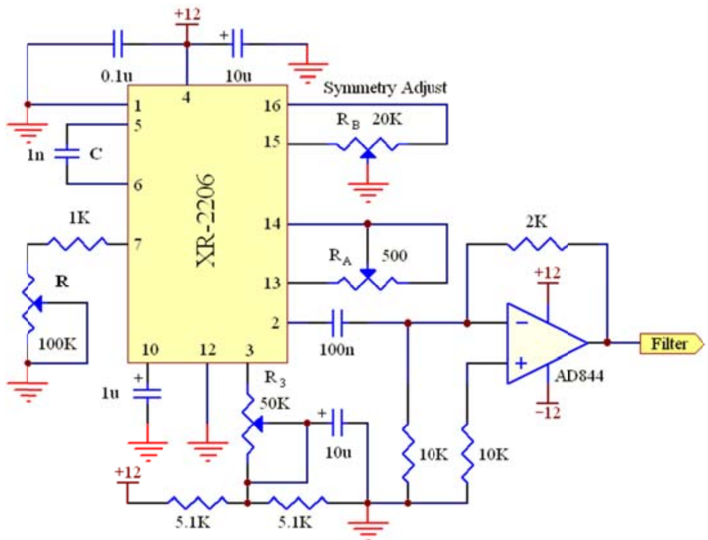

Fig. 4. Voltage-controlled oscillator (waveform generation part)

b) Butterworth band-pass filter

In order to have an exact waveform without any jitter, noise and distortion, and also to create low output impedance for the next stage (VCC), a Butterworth band-pass filter Ranging between 10KHz and 250KHz, has been designed and placed between the VCO and VCC parts of current source. Hence the operational frequency range of the designed EIT system would be between 10 and 250KHz. In order to design the filter for other frequencies, the Butterworth coefficients have been cited in [13]. The schematic circuit of the filter is shown in Fig. 5. As it is shown, the filter consists of a fourth-order Butterworth low-pass filter (U_1 and U_2) with cutoff frequency of 250 KHz and also a fourth-order Butterworth high-pass filter (U_4 and U_5) with a cutoff frequency of 10 KHz that are connected serially.

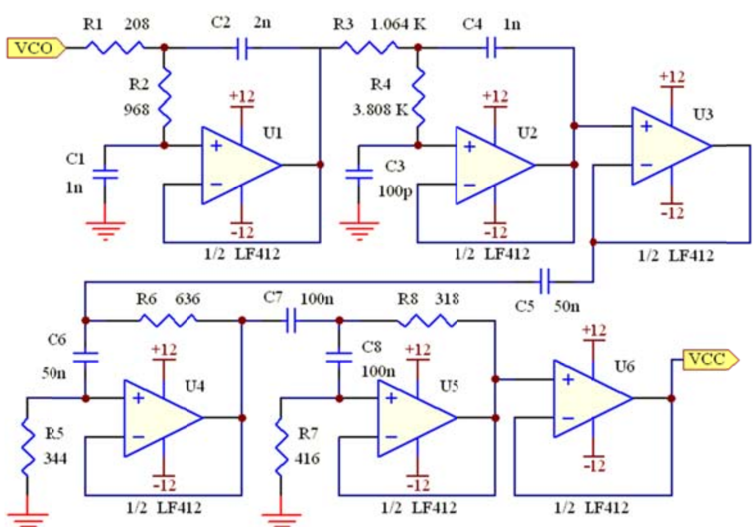

Fig. 5. Butterworth Band-pass filter which is put between the VCO and VCC parts

c) Voltage-to-current converter

The end structure of mentioned flowchart is Voltage-to-Current converter (VCC), many experiments were done to improve and modify its operation. Several essential tests were done on four main configurations of a VCCS:

- VCCS based on AH (Advanced Howland), [14, 15].
- VCCS based on DOA (Double-Operational Amplifier), [16].
- VCCS based on TOA1 (Triple-Operational Amplifier form 1), [17].
- VCCS based on TOA2 (Triple-Operational Amplifier form 2), [9].

These experiments were done with identical VCOs, different VCC structures, different component values such as different resistance values, different types of OP-AMP, and also different ranges of load. According to results of the primary practical tests, the best structure of the VCC part was selected and modified. The main selected criteria in the primary tests were based on the output impedance, the operational band-width, and the minimum and maximum loads that each VCCS can support. The schematic circuits of different VCCSs which have been used in practical tests and simulations (with PSPICE), and their results have been shown in Appendix A. Proposed structure of the VCC part with its components value, according to the best result in experiments is shown in Fig. 6. For VCCS based on TOA1 circuit, (2) should be satisfied and therefore I_L is calculated by (3).

$$I_L = \frac{\frac{R4}{R3+R4}Vi}{\left(\frac{R1}{R1+R2}-\frac{R3}{R3+R4}\right)RL + \frac{R1R5}{R1+R2}} \quad (1)$$

Here, if: $$\frac{R1}{R1+R2} - \frac{R3}{R3+R4} = 0\,, \quad \text{or} \quad R1\,.\,R4 = R2\,.\,R3 \quad (2)$$

We can get: $$I_L = \frac{R4}{R3\,.\,R5}.V_i \quad (3)$$

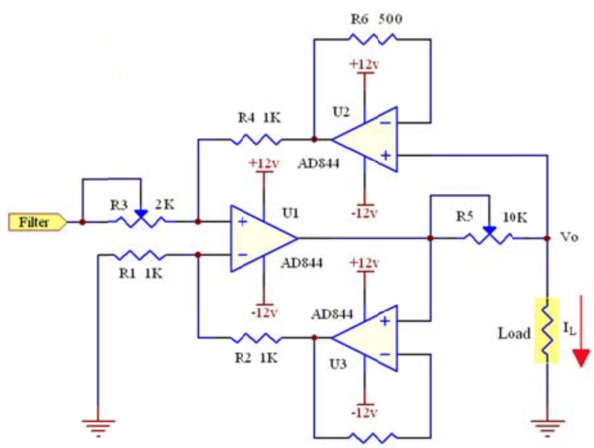

Fig. 6. Proposed structure of the VCC section, with suggested components values

The output impedance Z_{out} of a typical current source can be calculated by (4). As it is shown in Fig. 7, V_1 represents the measured output voltage of R_1, when the switch S is opened and V_2 represents the measured output voltage of R_1, when S is closed. R_P and R_1 are connected at the output of VCCS with optional value [2]. In order to measure the output impedance and also load voltage of a typical VCCS with an oscilloscope, the input impedance of the voltmeter (oscilloscope) should be considered.

$$Z_{out} = \frac{V1}{V2 - V1} \cdot R_P - R_1 \quad (4)$$

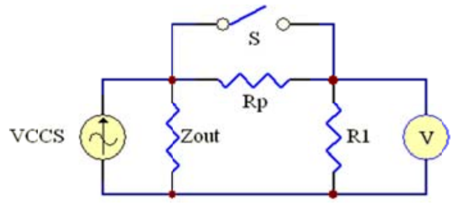

Fig. 7. A method for measuring VCCS output impedance [2]

Figure 8A shows the results of other practical tests to determine the best value for R_1 to R_4 according to the circuit of Fig. 6. In the curve, Maximum allowable load represents the maximum value of load in which the VCCS can support in a specific frequency. The output waveform of VCCS (load voltage) must be exact sinusoid and the relationship of the input voltage of VCC part and load current must be linear during the test. The amplitude of load current was adjusted on 1mA in all frequencies. In fact, the output Impedance of a current source depends on inverse of frequency [9]. The maximum allowable load in a particular frequency is also restricted by the value of output impedance. As a result according to the curve in Fig. 8A. The best value for R_1 to R_4 was selected as 1KΩ. This is due to the VCC structure with 1KΩ resistor, which creates higher output impedance compared to others.

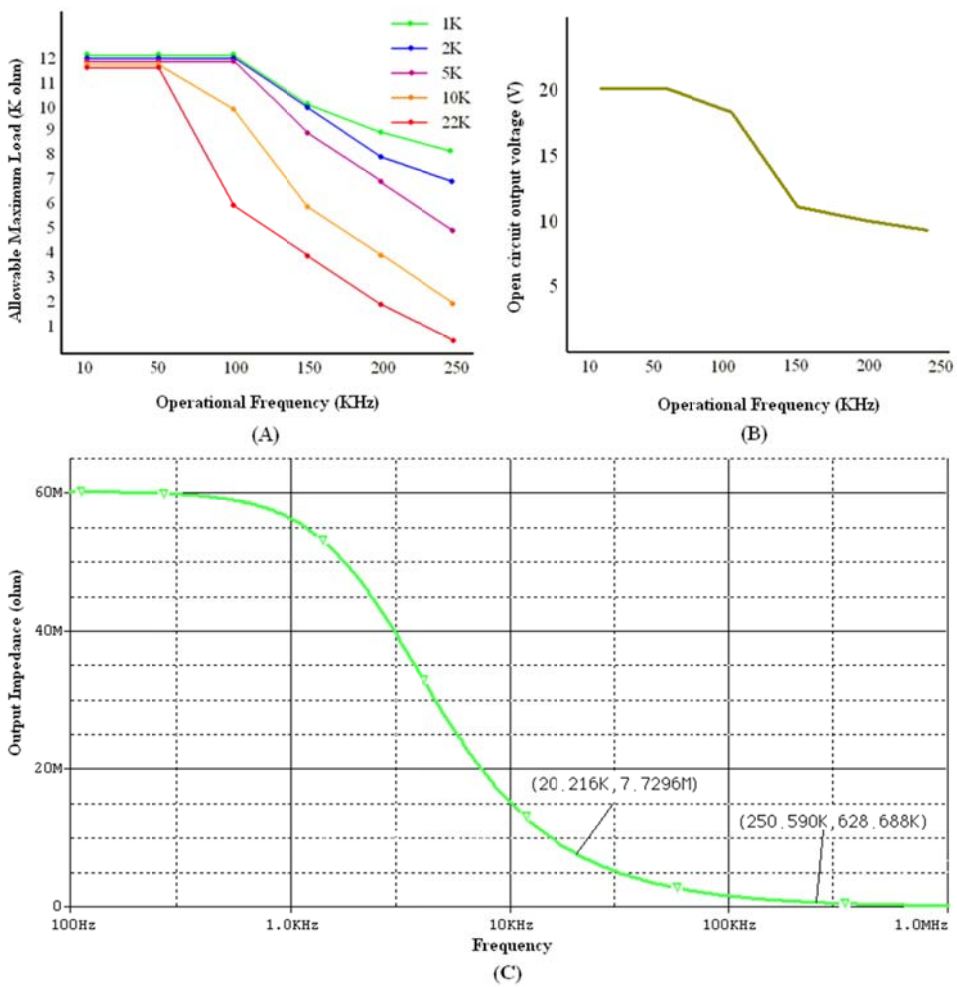

Fig. 8. (A) The curve represents the ranges of maximum allowable load which can be supported by the implemented VCCS, in different frequencies and different values of R_1 to R_4 according to the circuit in Fig. 6. (B) Open circuit output voltage of implemented VCCS in different frequencies. (C) Output Impedance of proposed VCCS, simulated with PSPICE in different frequencies

With this resistance value the maximum allowable load in frequencies less than 100KHz is 12KΩ which decreases to about 8KΩ in 250KHz as shown in the upper curve of Fig. 8A. The circuit in Fig. 6 was tested with resistors less than 1KΩ (~0.5KΩ), however, the waveform was distorted and the OP-AMPs were heated up. The result of the other practical test for the proposed VCCS is shown in Fig. 8B. In this part the output voltage of the VCCS was measured when there wasn't any load at the output of the circuit (open circuit voltage), in operational frequency range. Part C of Fig. 8 shows the output impedance of simulated VCCS in PSPICE.

d) Pulse generator

A pulse generation module has been attached to the VCCS circuit design in order to generate two types of synchronous pulse train with the maximum point of positive peaks and zero points of the output current waveform (peak detection and zero detection of the current).The pulses were used for demodulating the boundary voltages in order to measure them. Figure 9 shows the pulse generator circuit diagram. The input of the pulse generator is connected to the output of the filter. We may shift the position of the pulses with R_2. As shown in Fig. 10, sections A and B depict the worthwhile usage of this part. The pulse width can be varied by increasing C_1 from 1nF to 10nF. For instance, by regulating R_2, the output pulse train and also the signal of Point B may be used for sampling and extracting real part of the load voltage in the demodulator section.

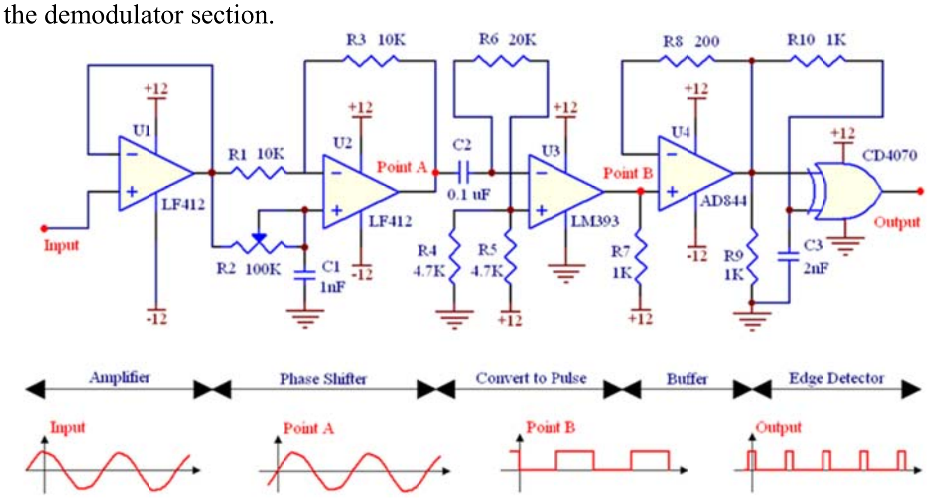

Fig. 9. Pulse generation schematic circuit

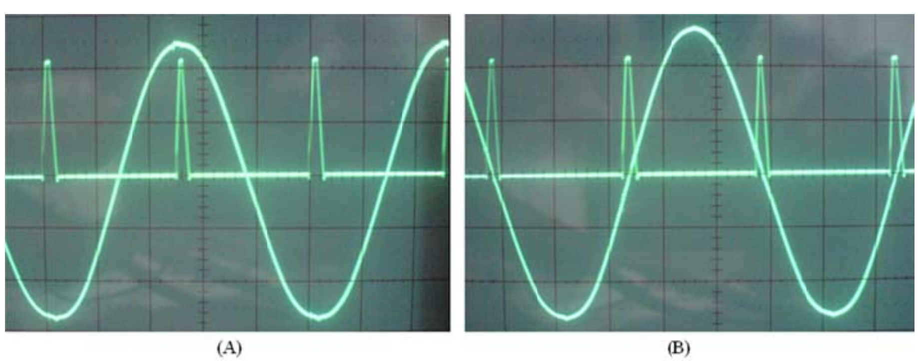

Fig. 10. The output generated pulses. (A) Peak detection (B) Zero detection

4. VOLTAGE MEASUREMENT

The data acquisition system can limit the overall accuracy [18]. Errors arise from both current drive and voltage acquiring parts of the EIT system. Related to the topology that is applied for measuring

(measuring pattern) in each moment, only one voltage can be measured via two particular electrodes. In addition to avoiding measurement error because of common mode effects, the voltage of electrodes which are connected to the current source is not measured.

a) Demodulation of electrodes voltage

In order to measure the boundary voltage, at first the electrodes voltage must be demodulated. At this stage, the voltage demodulator samples the voltage waveform in specific points and prepares sampled data for measurement. As an example, in order to measure the real portion of the load voltage, the samples should be taken from the load voltage when the injecting current would be on the maximum value of positive peak. On the mentioned points, the voltage of capacitance components of the subject is zero due to the 90 degree phase shift. The method of modulation is based on sample-and-hold approach that is known as pulse-sample demodulation. The suggested method does not require multiplier or output filter [19].

As it is shown in Fig. 11, both electrode voltages after passing through the high pass filters and buffers are entered to the high speed CMOS-logic analog multiplexers (74HC4053). The control pulses entered via ports C and D, come from the pulse generator part of the current source. To measure the real part of the load voltage, port C must be connected to the positive peak detector (point B of Fig. 11) and port D must be connected to the maximum point detector (to the output of the pulse generator part, when it works as the peak detector). Hence the input voltages of AD625 (programmable gain instrumentation amplifier) are the demodulated electrode voltages and the output voltage of the IC is differential value of those mentioned voltages. The gain value determined by R_7, R_8 and R_9 is optional and is calculated by (5) [20]. To measure the imaginary part of the load voltage the pulse of point B and zero detection output pulse should be applied as well.

$$R_7 = R_8 \qquad Gain = \frac{2R7}{R9} + 1 \tag{5}$$

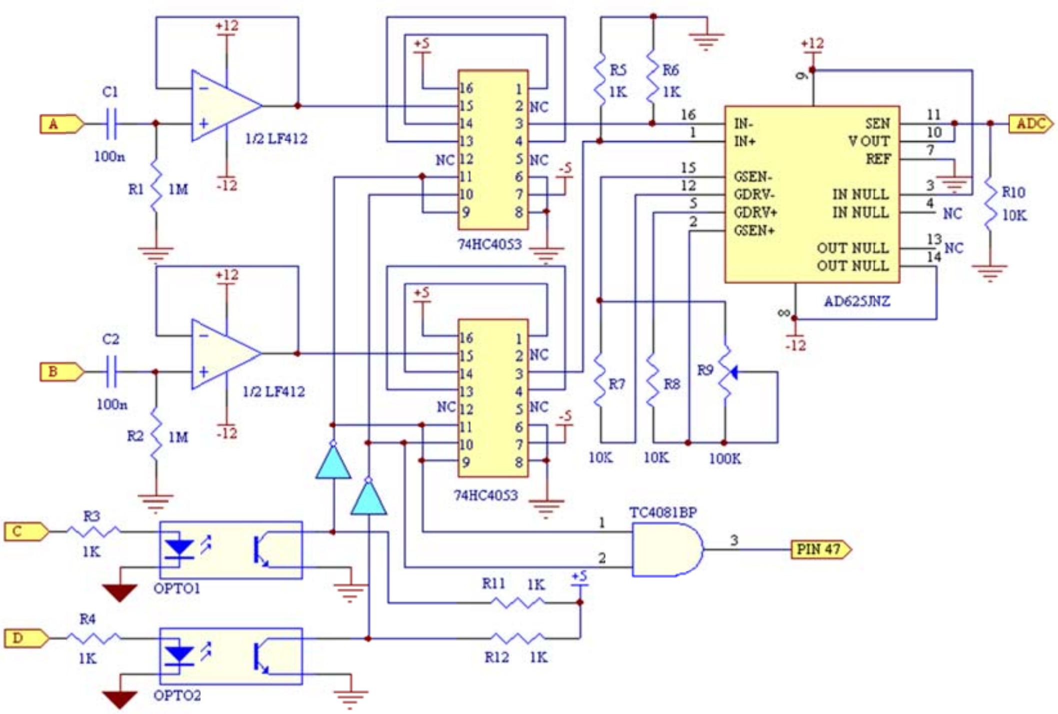

Fig. 11. Proposed design for demodulating of electrode voltages

b) Voltage measurement

At this stage the demodulated voltage is measured, hence it must be converted from analog to digital value. The digital value is then transmitted to the microcontroller (ATmega128) of control unit. In measurement part, AD1674 with 12-bit resolution is applied as an ADC. ATmega128 has a number of ADCs by itself, but its ADCs cannot be used in measurement. According to the data-sheet [21], the conversion time (i.e. required time for conversion of an analog value to valid digital data) of its ADCs, is between 13 to 260μs which is not an exact amount of time. So it would not be possible to capture the analog voltage signal at a specific point in the range of micro second. However, in AD1674, the conversion or sampling time is exactly 10μs [22], hence it is very interesting to capture the analog voltage whenever it is required. This is due to the 12-bit resolution of the IC, for amplitude between ±5V, the mentioned ADC can sense 2.44 mV changing on the analog voltage (one bit is used for sign).

5. MULTIPLEXER

A high-speed multiplexer module with 32 outputs can be added to the proposed instrumentation design. As it is seen in Fig. 12, the schematic circuit of the multiplexer module is illustrated. ADG506AKN is used as the analog multiplexer in our design.

For a 32-electrode EIT system, eight ICs of the mentioned multiplexer are required. Four of which are applied for injection and sink ports of current source and the others are used for voltage measurement. The multiplexer is applied for sharing the current source and voltmeter between multiple electrodes. For a 32-electrode system, 5 address lines are needed; hence four address lines of ADG506AKN plus its enable pin can be used. Each latch is applied for a pair of ADG506A (for lower and higher than 16 electrodes).

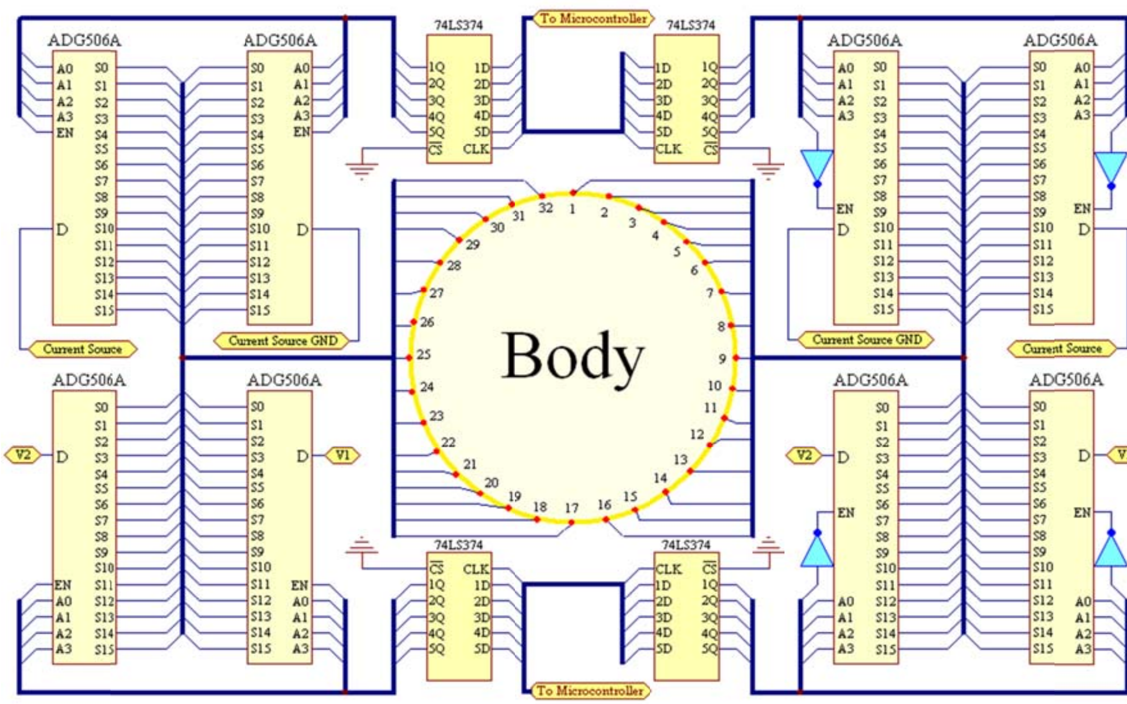

Fig. 12. The proposed design for multiplexer module

6. CONTROL UNIT

The control unit contains the following tasks:

- Controlling the multiplexer part to determine the state of each electrode on each moment.
- Communicating with a PC and matching with MATLAB for data transaction via RS-232.
- Connecting to LCD (if required), to display the voltages and also number of measurements.
- Connecting to ADC and controlling that as a slave with handshaking and interrupting signals.
- Communicating with AVR programmer for programming via ISP mode.

As it can be seen in Fig. 13, ATmega128 is applied as the microcontroller of control unit. All the output ports should be buffered to amplify the port output current and also to prevent the loading effect of the next stages.

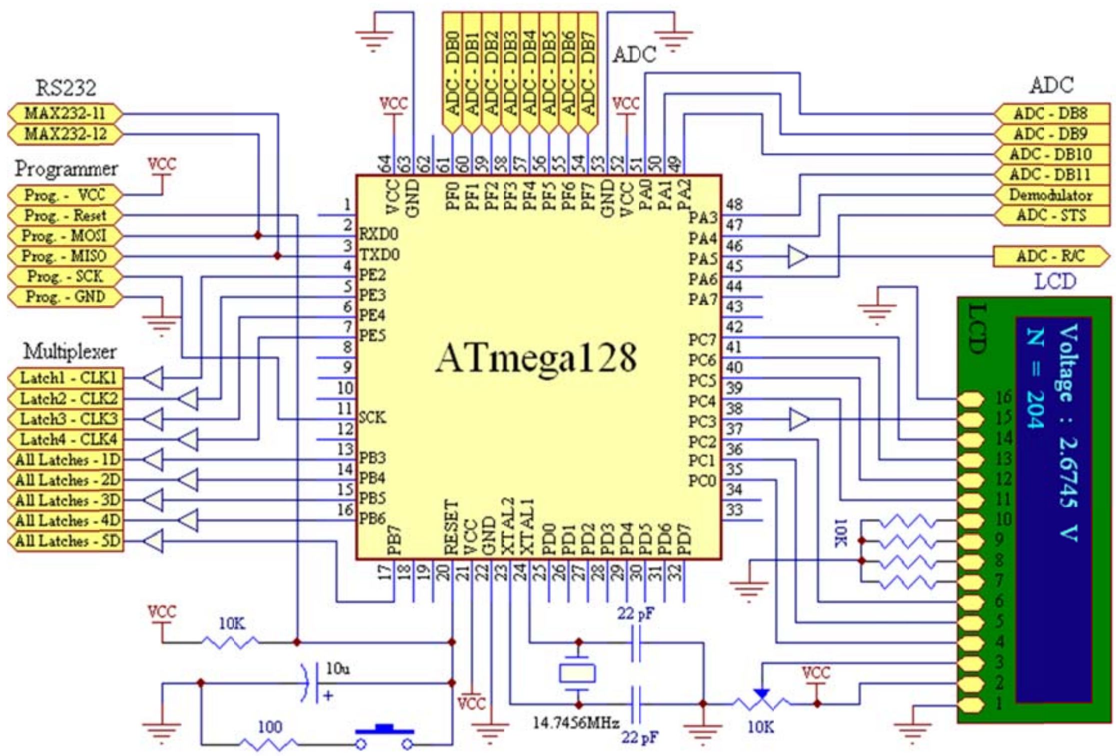

Fig. 13. The proposed design of control unit

a) Data transaction via RS-232

Serial communication is one of the protocols that are supported by many types of computer and therefore connecting the computer and microcontroller, RS-232 communication protocol is often applied [23]. After completion of the voltage measurement, the measured voltage stored in the microcontroller register must be transmitted to the computer. In the proposed EIT system, the microcontroller (ATmega128) is connected to the computer via MAX232, which converts the TTL voltage to RS-232 voltage and vice versa. Hence the data transaction is done by RS-232 serial communication via 9-pin COM port. In this design based on the standard frequencies and baud-rates (bps) table [23], the microcontroller frequency is assigned on 14.7456MHz. In the mentioned frequency for all standard baud-rates such as 2.4, 9.6 and 115.2 kbps, the data transaction error is zero.

7. STIMULATION AND MEASUREMENT PATTERNS

To show the experimental results of the proposed EIT system, different topologies can be used for stimulation (current injection) and voltage measurement, such as: adjacent pattern, opposite pattern and cross pattern. In this paper the adjacent pattern that is the most common pair-drive protocol [24] is applied as the stimulation and measurement topologies.

In the adjacent (neighboring) pattern, shown in Fig. 14, the current is applied through two adjacent electrodes and the voltages are measured from successive pairs of adjacent electrodes. The current is then applied through the next pair of electrodes, and the voltage measurements will be repeated for others. The procedure will be continued until each possible pair of adjacent electrodes is used to inject current. In this pattern, it is common to use all $N \times (N - 3)$ measurements in most reconstruction algorithms, where N is the number of electrodes. ATmega128 in the control unit has been programmed based on the adjacent pattern as the system stimulation and measurement protocols. In this pattern the current is injected mainly in the outer region of the imaged object. The current density is highest between the injecting electrodes, and decreases rapidly as a function of distance.

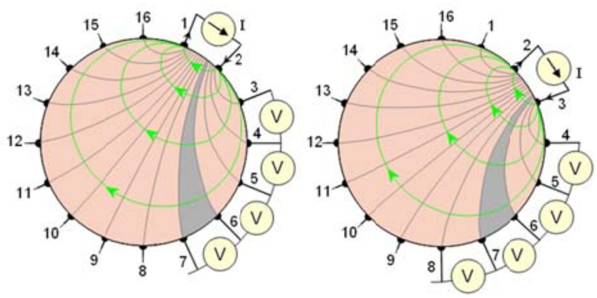

Fig. 14. Adjacent pattern as the stimulation and measurement protocols of the proposed EIT system

8. EXPERIMENTAL RESULTS

To evaluate performance of the system to reconstruct images, some experiments were carried out on the cylindrical phantom with a few test objects. The images reconstructed by using the implemented system will be shown and described, and some elements that can affect the quality of images will be introduced. In all experiments, the saline used in phantoms is prepared with solution of NaCl and de-ionized distilled water. A current signal (~1mA) with 20 KHz frequency is injected to the boundary of phantoms via two electrodes. Adjacent pattern is used as the stimulation and voltage measurement protocol in all experiments. All images are reconstructed by using the Eidors MATLAB package [25, 26]. The cylindrical phantom is made of Plexiglas with a radius of 15cm.

a) Experiment 1

In the first experiment two pieces of a plastic (Teflon) shaft have been placed in front of electrode 1 of a 16-electrode cylindrical phantom. The aim of experiment is to evaluate the quality of reconstructed image of subjects having less conductivity than saline. The reconstructed images of this phantom are shown in Fig. 15. Parts B, E and F show the fine-model images of phantom, and the coarse models are illustrated in parts C and D. In parts B, D, and F the image of phantom, is reconstructed onto nodes, but in parts C and E the image is reconstructed onto elements.

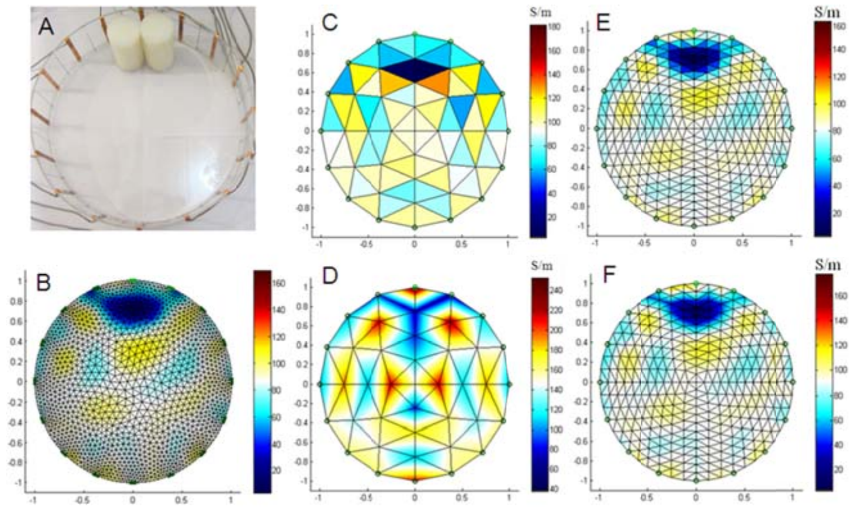

Fig. 15. (A) Phantom with two pieces of plastic shaft. (B) Fine model reconstructed onto nodes. (C) Coarse model reconstructed onto elements. (D) Coarse model reconstructed onto nodes. (E) Fine model reconstructed onto elements. (F) Fine model reconstructed onto nodes

b) Experiment 2

In this experiment, two pieces of a metallic (Aluminum) shaft have been placed in front of electrodes 4 and 14 of a 16-electrode cylindrical phantom with 30 cm diameter. The aim of this test is to understand the quality of reconstructed image of the subjects having as much conductivity as saline. Parts B to F of Fig. 16 illustrate the final reconstructed images of the phantom (shown in part A) by using different fine and coarse mesh generation models.

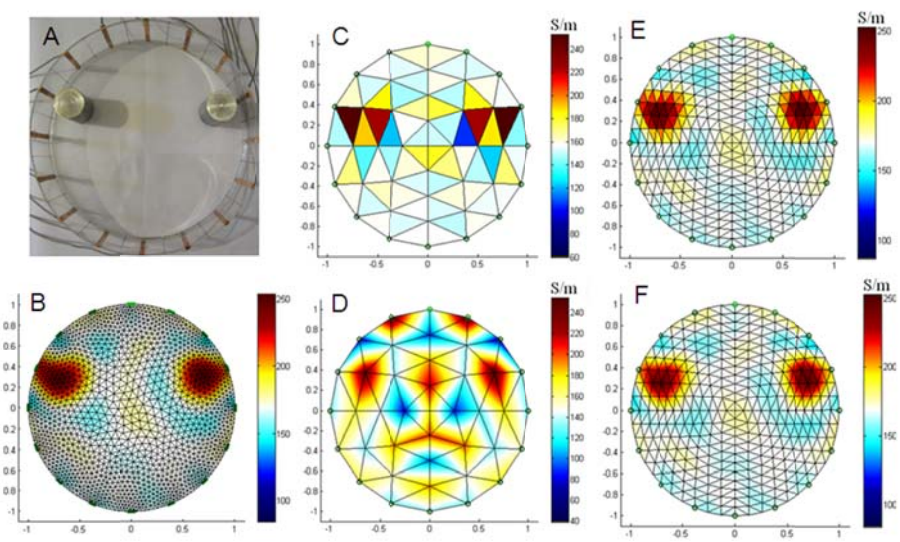

Fig. 16. (A) Phantom with two pieces of metallic shaft. (B) Fine model reconstructed onto nodes. (C) Coarse model reconstructed onto elements. (D) Coarse model reconstructed onto nodes. (E) Fine model reconstructed onto elements. (F) Fine model reconstructed onto nodes

c) Experiment 3

In this experiment, four pieces of the metallic and plastic shafts have been put in the 16-electrode cylindrical phantom. The experiment is conducted to evaluate the quality of reconstructed image of the subjects in different conductivities locating in composite setting. The final reconstructed images in fine and coarse models are shown in parts B to F of Fig. 17.

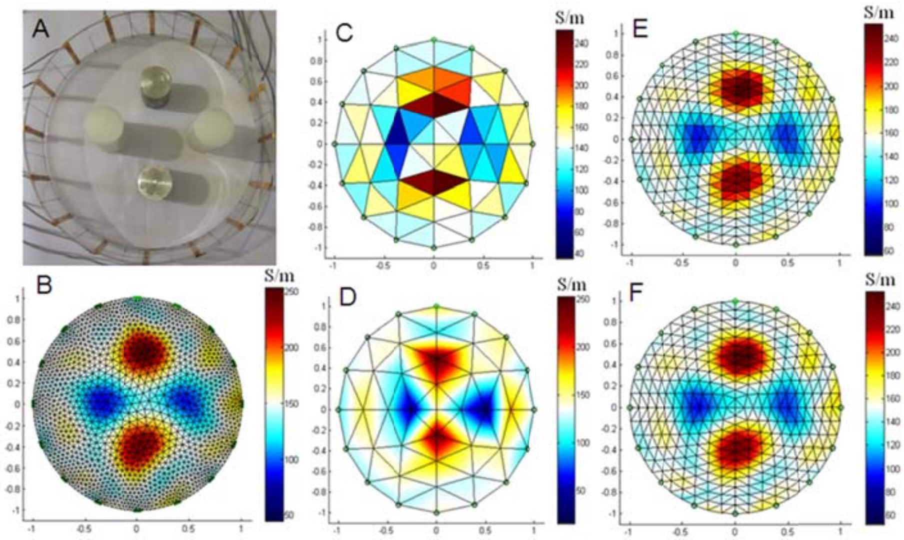

Fig. 17. (A) Phantom with four pieces of metallic and plastic shafts. (B) Fine model reconstructed onto nodes. (C) Coarse model reconstructed onto elements. (D) Coarse model reconstructed onto nodes. (E) Fine model reconstructed onto elements. (F) Fine model reconstructed onto nodes

d) Experiment 4

In the following, three plastic and metallic subjects have been placed in a 16-electrode thorax-shape phantom. The goal of this test is evaluation of quality of the images reconstructed by using a 16-electrode thorax-shape phantom. As it can be seen in Fig. 18B, the image is reconstructed onto elements, but in part C (of Fig. 18) the image is reconstructed onto nodes.

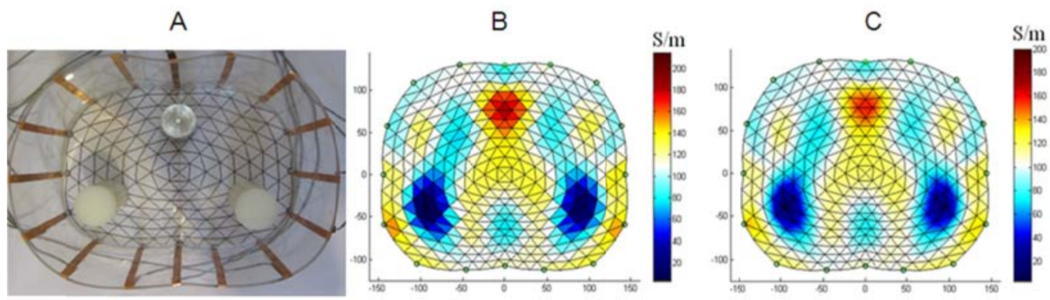

Fig. 18. (A) A 16-electrode thorax-shape phantom with some subjects. (B) Fine model reconstructed onto elements. (C) Fine model reconstructed onto nodes

e) Experiment 5

The aim of conducting this experiment is to show the effects of hyper-parameter (λ) in reconstructed images, and evaluate the quality of the final images reconstructed with different values of hyper-parameter. In fact hyper-parameter (λ) is a scalar that controls the amount of regularization. The goal of hyper-parameter selection is to produce the best reconstruction with high quality and resolution. Hyper-parameter selection should produce solutions that preserve as much of the measured data as possible to obtain a useful reconstruction [24]. Practically in image reconstruction, insufficient hyper-parameter causes the image to be dominated by noise and as it is increased, noise is filtered through the smoothing action. As it can be seen in Fig. 19, few reconstructed images of the phantom with different hyper-parameter values are shown. Obviously the reconstructed image with $\lambda = 0.01$, represents the best image in terms of precision and quality.

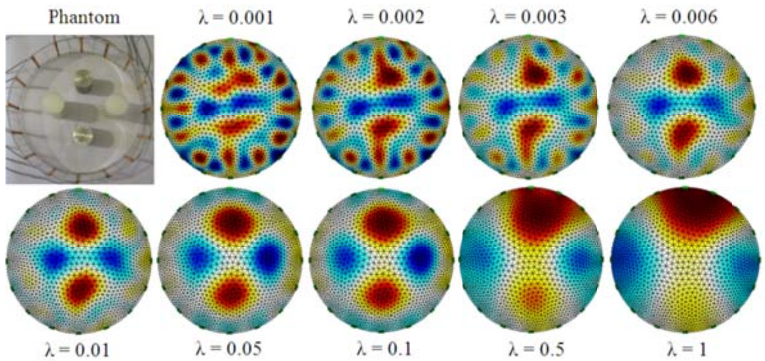

Fig. 19. Some images which were reconstructed with different λ values (hyper-parameter) by using the 16-electrode EIT system. The image with λ=0.01 represents the best image in terms of precision and quality

f) Experiment 6

In the current experiment, effect of number of voltage frame or number of scanning in the reconstructed image quality will be analyzed. In fact, in adjacent pattern the number of voltages in each frame acquired by scanning an N-electrode phantom is calculated by $N\times(N-3)$. Hence after scanning a 16-electrode phantom each frame of voltage contains 208 voltages.

In experiment 6 some metallic and plastic subjects are located in different positions of a 16-electrode cylindrical phantom as shown in Fig. 20.A. The image in part B is reconstructed by using only one frame of voltage which means that the image is reconstructed after one time scanning, therefore some effects of noise can be seen on this image (near electrodes 4, 8, 9, and 10). However the image in part E is reconstructed after scanning ten times, which means image reconstruction is done using the average of ten frames of voltages. So the effects of noise are improved in the mentioned image. The images in parts C and F of Fig. 20 are the 3D images of the phantom of part A, which are reconstructed by different number of voltage frames. The image in part F reconstructed after scanning ten times is smoother than the image of part C which is reconstructed after scanning only one time. This result can be extracted so that, by using the average of voltage frames instead of one frame, in image reconstruction process, the quality of the final reconstructed images would be improved.

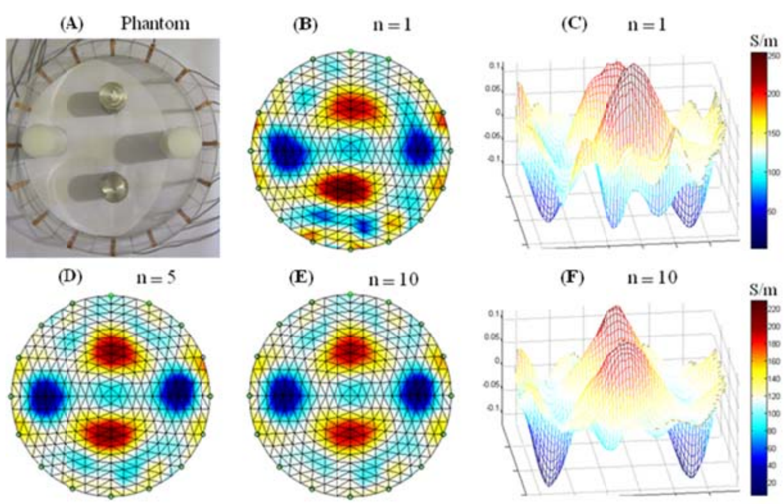

Fig. 20. Some reconstructed images of one phantom, by using the average of **n** voltage frames. (A) Phantom with four pieces of metallic and plastic shafts. (B) n=1. (C) 3D image (3D surface plot) of phantom in part A with n=1. (D) n=5. (E) n=10. (F) 3D image of phantom in part A with n=10

g) Experiment 7

The objective of experiment 7 is to show the effects of number of electrodes in the final reconstructed image quality. To evaluate the image quality, three positions of a phantom surface would be considered: near the boundary, in the central part and the whole phantom (both central part and near the boundary). In this test, three phantoms are applied with different numbers of electrodes which are 8, 16 and 32 electrodes. The dimensions of phantoms and internal saline and subjects are identical. First position for evaluation is near the boundary. As it can be seen in Fig. 21, the distance between subjects to the inner wall of the phantoms is about 2~3 cm, but in the reconstructed images by 8-electrode and 16-electrode phantoms, in some places show that the dark parts (smudges) are connected to the boundary of image, whereas in reconstructed images by 32-electrode phantom as it can be seen, the dark parts are completely separated from the boundary of phantoms.

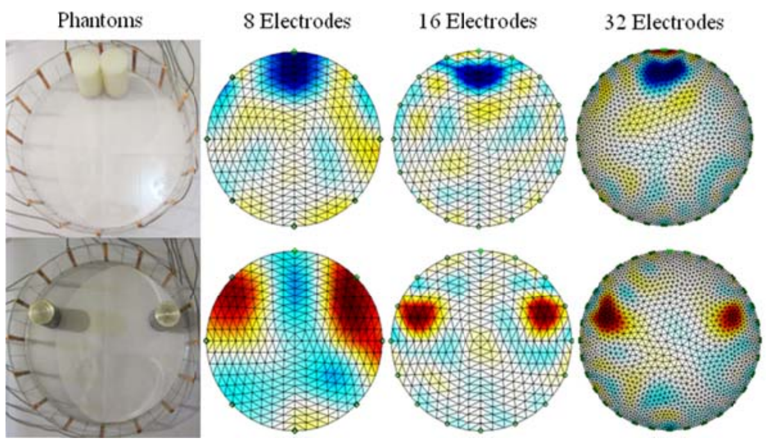

Fig. 21. Reconstructed images of subjects which are located near the boundary of phantoms with various numbers of electrodes to show their accuracy in final image reconstruction quality

The next position is the central part of the phantom. As is illustrated in Fig. 22, the quality of reconstructed image of subjects put in the central part is poor. This is because the pattern which was applied as the stimulation and measurement topologies in all image reconstructions in this paper is Adjacent pattern, and it is very sensitive to conductive parts near the boundary and insensitive to the central parts. It is sensitive to disturbances in the boundary shape of the object, the position of the electrodes, measurement error and noise as well [24, 27].

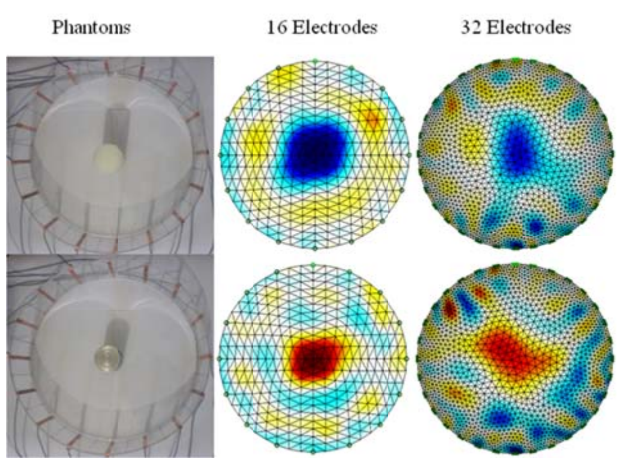

Fig. 22. Showing quality of reconstructed images of the subject, which is located in central part of phantoms, by means of various numbers of electrodes

The last position is the whole phantom. As shown in Fig. 23, the reconstructed image of the 8-electrode phantom is very crude, and it does not have acceptable accuracy to show the correct position of the subjects which are located in the phantom. But despite the bad quality and showing inexact position of the subjects, there is a dark smudge in the central part of this image, as the position of the central plastic shaft. But it cannot be seen in the reconstructed image of 32-electrode phantom. The reconstructed image of the 16-electrode phantom shows the correct position of the subjects located near the boundary, but instead of the central plastic shaft it shows a very light smudge.

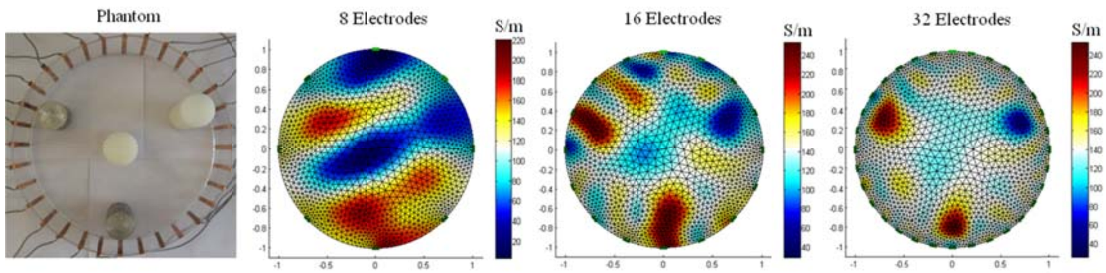

Fig. 23. Reconstructed images of three phantoms with different numbers of electrodes. Subjects are located in different positions of the phantom (central part and near the boundary), and these positions were identical in three reconstruction processes

The reconstructed image of the 32-electrode phantom also exactly shows the correct position of subjects located near the boundary, but it does not show anything, even a light smudge, in its central part instead of plastic shaft!

Hence the result that can be acheived from this experiment is, for an EIT system that works based on the adjacent pattern, when the number of electrodes of phantom increases, the system sensitivity to the parts near the boundary will be increased, but its sensitivity to the central part of the phantom will be decreased specifically when some subjects have been located near the boundary. The reason of this phenomenon is that in 8-electrode phantom the distance between electrodes is more than the others (16 and 32-electrode phantoms), and it causes more current density in the central part, which results in more sensitivity. Therefore in image reconstruction accuracy, related to measurement and stimulation topologies, the position of subjects is important as well, even when using 32-electrode system.

9. VISUAL COMPARISON ON RESOLUTION

Although the EIT has been developed substantially over recent years, there are many challenges (such as resolution) that still need to be overcome to make it a clinically applicable imaging [28]. EIT has been extensively researched in clinical diagnosis [29, 30], but due to poor Signal to Noise Ratio (SNR) of the boundary voltage data and poor spatial resolution of image, the EIT systems have not yet been accepted as regular medical imaging devices.

In this part, the quality of reconstructed image using the proposed EIT system will be compared visually with quality of images produced by using other implemented EIT systems. The other EIT systems include an EIT system proposed by Bera and Nagaraju in [31] and a DSP based multi-frequency EIT system designed by Goharian et al in [32]. In fact in both systems, image is reconstructed by using a 16-electrode phantom and from this point of view those systems are similar to the proposed system. The test objects located in phantoms are made from similar materials (plastic and metal) as well.

As a matter of fact, the size of all phantoms and test objects are different in comparison with each other, but the size and position of subjects in their own phantoms are exactly plotted in the middle column of Fig. 24 according to their paper information [31-32]. The mapped image of phantoms and their inner objects (in middle column of Fig. 24), have been drawn with the exact proportion compared to dimensions of real phantoms and their containers applied in image reconstruction. As it can be seen in Fig. 24, the first column shows three 16-electrode phantoms related to different EIT systems containing saline and test objects. The third column shows the reconstructed images made by three different EIT systems. The quality or resolution of reconstructed image seen in Fig. 24.C is obtained by using only 16 electrodes from 32 electrodes of the implemented EIT system. Of course, the quality and resolution of image will be increased if the number of electrodes increases.

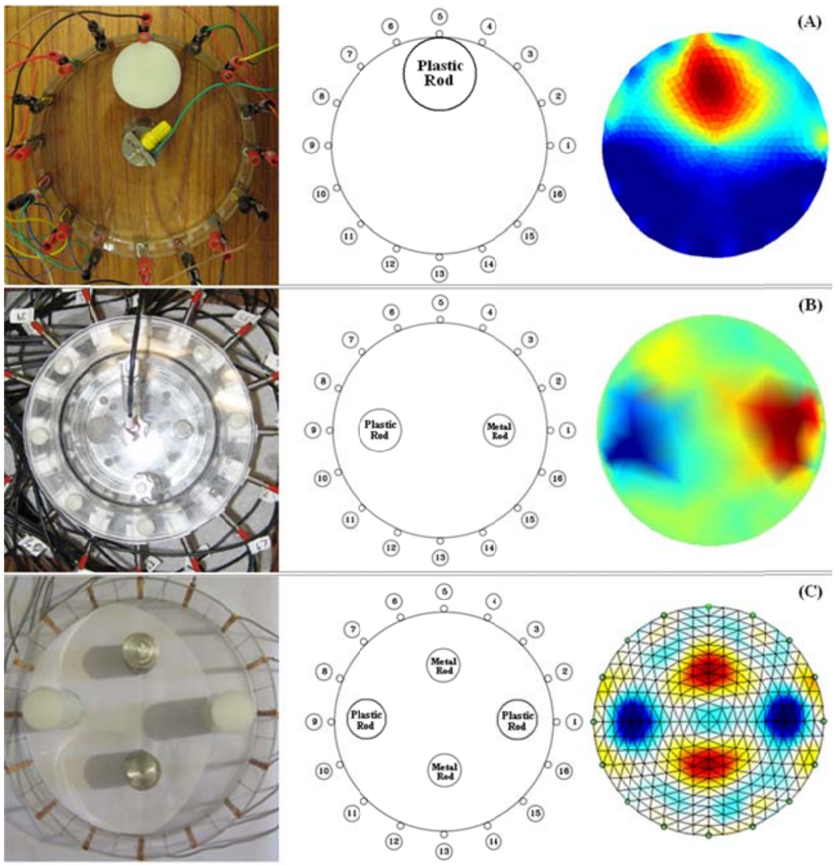

Fig. 24. Visual comparison on quality of final images made by applying three different implemented EIT systems. (A) reconstructed image by using EIT system proposed by Bera and Nagaraju in [31]. (B) reconstructed image by using a DSP based multi-frequency EIT system proposed by Goharian et al in [32]. (C) reconstructed image by using our EIT system

9. CONCLUSION

In this paper a practical low-cost precise design of EIT instrumentation was proposed and described in detail. System performance has been checked with a saline tank and some experimental results have been shown. The novelty of this design is its precision which was achieved without any complex circuits. Simplicity of design made it possible to have a low-cost instrumentation which could pave the way for EIT researchers for designing and implementation of EIT hardware. Some hard work has been done from the practical point of view to improve the precision of the proposed system such as trying to maximize the output impedance of the current source, which was finally increased to more than 5 MΩ such that it wasn't possible to be measured with oscilloscope. Higher quality of the reconstructed images by our system with 16 electrodes compared to the others is the best reason to verify the accuracy of the implemented EIT hardware. Future research includes improvement of the current EIT hardware in terms of accuracy and precision to become appropriate for clinical applications and development of EIT application in industrial and medical fields.

REFERENCES

1. Horesh, L. (2006). Some novel aproches in modelling and image reconstruction for multi-frequency electrical impedance tomography of the human brain. *PhD thesis*.
2. Denyer, C. W. L. (1996). Electronics for real-time and three-dimensional electrical impedance tomography. *PhD thesis*.
3. Yan, W., Hong, S. & Chaoshi, R. (2006). Optimum design of electrode structure and parameters in electrical impedance tomography. *Physiol. Meas.,* Vol. 27, pp. 291-306.
4. Boone, K. G. & Holder, D. S. (1996). Current approaches to analogue instrumentation design in electrical impedance tomography. *Physiol. Meas.17(suppl 1A) A229–A247*.
5. Murphy, S. C., Chin, R. K. Y. & York, T. A. (2008). Design of an impeller-mounted electrode array for EIT imaging. *Meas. Sci. Technol*., Vol. 19, pp. 1-12.
6. Goharian, M., Soleimani, M., Jegatheesan, A., Chin, K. & Moran, G. R. (2008). A DSP based multi-frequency 3D electrical impedance tomography system. *Ann. Biomed. Eng*., Vol. 36, pp. 1594-1603.
7. Yorkey, T. J. (1986). Comparing reconstruction methods for electrical impedance tomography. PhD thesis, University of Wisconsin at Madison, Madison, WI 53706.
8. Filho, B., Brown, B. H. & Wilson, A. J. (2000). A comparison of modified Howland circuits as current generators with current mirror type circuits. *Physiol.Meas.,* Vol. 21.
9. Holder, D. S. (2005). *Electrical impedance tomography: methods, history and applications (Series in Medical Physics and Biomedical Engineering)*. Institute of Physics Publishing Ltd.
10. Khalighi, M., Vosoughi Vahdat, B., Mortazavi, M. & Soleimani, M. (2012). Practical design of low-cost instrumentation for industrial Electrical Impedance Tomography (EIT). *IEEE I2MTC*, Graz.
11. Zhao, D. (2011). High output-impedance current source for electrical impedance tomography. *IEEE 4th International Conference on Biomedical Engineering and Informatics (BMEI)*.
12. Denyer, C., Lidgey, F. & Zhu, Q. (1994). A high output impedance current source. *Physiol. Meas*., Vol. 15, pp. A79-A82.
13. Kugelstadt, T. (2009). *Active filter design techniques (chapter 20), Excerpted from OP AMPs for everyone*. literature number: SLOD006A, published by Texas Instruments, third edition.
14. Cusick, G., Holder, D. S., Birkett, A. & Boone, K. (1994). A system for impedance imaging epilepsy in ambulatory human subjects. *Innov. Tech. Biol. Med.15(suppl 1A) A33–A39*.
15. Jossinet, J., Tourtel, G. & Jarry, R. (1994). Performance and operation of a set of wideband current generators for EIT. *Innov. Tech. Biol. Med. 15(suppl 1A) A40–A46*.
16. Zhang, Y. L., Zhui, X., Chaoshi, R., Wei, W., Dechun, Z. & Huiquan, Z. (2010). Study of voltage controlled current source in electrical impedance tomography system. *IEEE, iCBBE, 4th Int. Conference*.
17. Shuai, Z., Guizhi, X., Huanli, W. & Duyan, G. (2006). Multi-frequency EIT hardware system based on DSP. *IEEE EMBS, 28th Annual international conference, China*.
18. Smith, R. W. M. (1990). Design of a real-time impedance imaging system for medical applications", *PhD Thesis, University of Sheffield*.
19. Soleimani, M. (1998). Designing and making the electrical impedance tomography systems. *Sharif University of Technology, Msc thesis*.
20. Data-sheet, (2000). *AD625, programmable gain instrumentation amplifier*. Analog Devices Inc., USA.
21. Data-sheet, (2006). *ATmega128, 8-bit AVR microcontroller with 128K bytes programmable flash*. Atmel Inc.

22. Data-sheet, (2000). *AD1674, 12-bit 100 kSPS A/D converter*. Analog Devices Inc., USA.
23. Rahafrooz, A. (2009). *AVR Microcontrollers and their applications*. Nas publishing.
24. Graham, B. M. (2007). Enhancements in Electrical Impedance Tomography (EIT) image reconstruction for 3D lung imaging. University of Ottawa. PhD thesis, Degree in electrical and computing engineering.
25. Vauhkonen, M., Lionheart, W. R. B., Heikkinen, L. M., Vauhkonen, P. J. & Kaipio, J. P. (2001). A MATLAB package for the EIDORS project to reconstruct two dimensional EIT images. *Physiol. Meas*., Vol. 22.
26. Adler, A. & Lionheart, W. R. B. (2006). Uses and abuses of EIDORS: an extensible software base for EIT. *Physiol. Meas.*, Vol. 27.
27. Dickin, F. & Wang, M. (1996). Electrical resistance tomography for process applications. *IOP Science, Measurement Science and Technology*, Vol. 7, No. 3, pp. 247-260.
28. Bayford, R. H. (2006). Bioimpedance tomography (Electrical impedance tomography). *Annual Review of Biomedical Engineering*, Vol. 8, pp. 63-91.
29. Brown, B. H. (2001). Medical impedance tomography and process impedance tomography: a brief review. *IOP Science, Measurement Science and Technology*, Vol. 12, No. 8, pp. 991–996.
30. Hoetink, A. E., Faes, T. J. C., Marcus, J. T., Kerkkamp, H. J. J. & Heethaar, R. M. (2002). Imaging of thoracic blood volume changes during the heart cycle with electrical impedance using a linear spot-electrode array. *IEEE Transaction on Medical Imaging*, Vol. 21, Issue 6.
31. Bera, T. K. & Nagaraju, J. (2011). Resistivity imaging of a reconfigurable phantom with circular inhomogeneities in 2D-electrical impedance tomography. *Elsevier, Measurement*, Vol. 44, pp. 518-526.
32. Goharian, M., Soleimani, M., Jegatheesan, A., Chin, K. & Moran, G. R. (2008). A DSP based multi-frequency 3D electrical impedance tomography system. *Annals of Biomedical Engineering*, Vol. 36, No. 9.
33. Khalighi, M., Vosoughi Vahdat, B. & Mortazavi, M. (2011). Designing a practical high output impedance current source for EIT systems. *IJRTET*, Vol. 6, No. 2, DOI: 01.IJRTET.06.02. 239.

APPENDIX A. SCHEMATIC CIRCUITS OF MENTIONED VCCSS AND THE RESULTS OF PRIMARY PRACTICAL TESTS

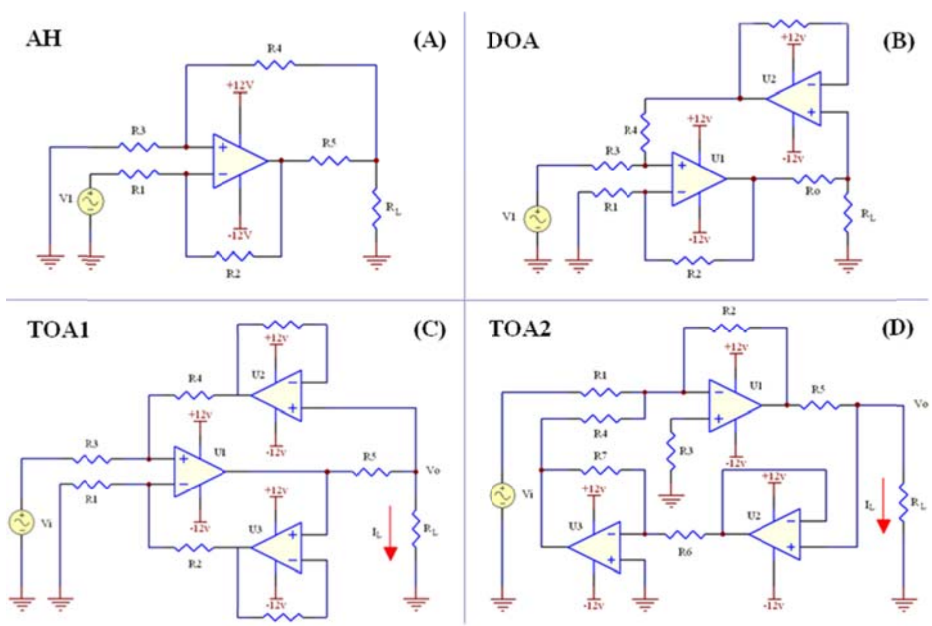

Fig. A1. (A) VCCS based on Advanced Howland [14, 15]. (B) VCCS based on Double-Operational Amplifier [16]. (C) VCCS based on Triple-Operational Amplifier form 1 [17]. (D) VCCS based on Triple-Operational Amplifier form 2 [9]

Figure A1 shows different schematic circuits of the VCCS which have been used in practical tests. As it can be seen in Table A1, the results of several experiments are shown briefly. These tests were done on the breadboard with different resistance values in condition of 20KHz frequency and 1mA load current. It can be concluded (from Table A1) that the VCCS based on TOA1 (fourth row) is the best choice to have an efficient voltage-controlled current source. It can support a load in range of 10Ω to 10KΩ linearly and also has more than 5MΩ output impedance which calculated with (4).

Table A1. The results of VCCS primary physical tests [33]

VCCS Type	R_1 (KΩ)	R_2 (KΩ)	R_3 (KΩ)	R_4 (KΩ)	R_5 (KΩ)	Allowable Load (Ω)	Measured Z_{out} (Ω)	PSPICE Z_{out} (Ω)
AH	1	2	1	1	1	10 ~ 1K	100K	420K
DOA	1	1	1	1	5	10 ~ 5K	3 M	5.3M
TOA1	1	1	1	1	5	10 ~ 10K	>5 M	7.8M
TOA1	2	2	2	2	5	10 ~ 10K	1 M	3.9M
TOA1	5	5	5	5	5	10 ~ 10K	500K	1.6M
TOA1	10	10	10	10	5	10 ~ 10K	500K	770K
TOA1	22	22	22	22	5	10 ~ 10K	150K	340K
TOA1	27	27	27	27	5	10 ~ 10K	100K	280K
TOA2	1	1	1	1	5	10 ~ 10K	600K	2.5M